Journal of Structural Geology 30 (2008) 1372–1382

Contents lists available at ScienceDirect

Journal of Structural Geology

journal homepage: www.elsevier.com/locate/jsg

Strain localization in direct shear experiments on Solnhofen limestone at high temperature – Effects of transpression

Sergio Llana-Fúnez*, Ernest H. Rutter

School of Earth, Atmospheric and Environmental Sciences, University of Manchester, Oxford Road, M13 9PL Manchester, UK

ARTICLE INFO

Article history:
Received 20 February 2008
Received in revised form 15 July 2008
Accepted 15 July 2008
Available online 30 July 2008

Keywords:
Experimental direct shear testing
Transpressional deformation
Strain heterogeneity
Plastic flow
Shear localization
EBSD

ABSTRACT

Some features of natural shear zones formed under non-coaxial strain geometries, including some effects of transpression, can be simulated in the laboratory by using the direct shear experimental configuration. Slices of ~1 mm thick Solnhofen limestone were deformed in direct shear between two stronger forcing blocks of cores of Tennessee sandstone pre-cut at 45° to the cylinder axis. Experiments were run dry at 600 °C, 200 MPa confining pressure and bulk shear strain rates of $\sim 5 \times 10^{-3}\ s^{-1}$, at which conditions Solnhofen limestone deformed by dislocation creep with a stress exponent of 4.7. When loaded, strain concentrates in the limestone band, producing non-coaxial deformation as one pre-cut block slides past the other. The orientation and intensity of the shape fabric developed in calcite grains indicate that strain is heterogeneous across the specimen, with the formation of two high-strain shear bands close to the limestone–sandstone interface, separated by a central zone of low strain. Crystallographic preferred orientation patterns in the calcite grains measured by electron backscatter diffraction are consistent with a switch in deformation geometry from flattening-dominated in the middle of the specimen towards shear-dominated in the high-strain bands. From tests on thin slices of the same material compressed axisymmetrically (without shearing) normal to the layer, heterogeneous thinning of the slice develops, from a maximum in the centre of the slice to zero at the edges. The formation of the paired shear zones observed in the sheared experiments is interpreted in terms of superposed strain fields, with shearing in the centre of the slice being inhibited by the strain hardening that accompanies the higher flattening strain in the centre of the specimen.

1. Introduction

The direct shear experimental configuration has often been used in experimental rock deformation studies to simulate a natural shear zone. In a conventional 'triaxial' testing machine it uses two cylindrical forcing blocks of a strong material cut at an angle such as 45° or 30° to the maximum compression direction, and sandwiching a thin slice of weaker 'target' homogeneous rock material in-between (e.g. Jaeger and Cook, 1976; Fig. 1). A length/thickness ratio sufficiently large to resemble a tabular geometry (>10:1; Fig. 1) makes the experimental configuration somewhat analogous to shear zones in nature (Ramsay and Graham, 1970; Ramsay and Huber, 1983, 1987). Axisymmetric loading along the length of the specimen assembly at high confining pressure will make one of the forcing blocks slide pass the other. By using rigid forcing blocks and ensuring that slippage at the interfaces is prevented, all strain will be accommodated in the tabular specimen. This procedure has previously been used successfully in a number of seminal papers that reproduced structures and microstructures characteristic of shear zones in naturally deformed rocks, particularly those microstructures indicative of non-coaxial deformation (e.g. Shimamoto and Logan, 1981; Schmid et al., 1987; Dell'Angelo and Tullis, 1989; Logan et al., 1992; Post and Tullis, 1999). It has also been used to infer rheological properties of natural and synthetic rocks fabricated by hot-pressing, although it has the major disadvantage that attainable bulk shear strains are limited, e.g. maximum bulk shear strain γ in the ~1–5 range can be attained, according to how thin the specimen can be made (Schmid et al., 1987; Mariani et al., 2006).

Despite the finite lateral extent of the thin, tabular form of specimens deformed using this geometry, it has been common to neglect any effects of thinning and lateral extrusion of sample material, particularly when initially non-porous samples of intact material are used. Shearing deformation accompanied by lateral extrusion and thinning of the specimen corresponds to tectonic transpression, that has often been invoked to explain complex

* Corresponding author. Present address: Department of Earth and Ocean Sciences, University of Liverpool, 4 Brownlow Street, L69 3GP Liverpool, UK. Tel.: +44 151 794 5145; fax: +44 151 794 5196.
E-mail address: s.llanafunez@liverpool.ac.uk (S. Llana-Fúnez).

0191-8141/$ – see front matter © 2008 Elsevier Ltd. All rights reserved.
doi:10.1016/j.jsg.2008.07.004

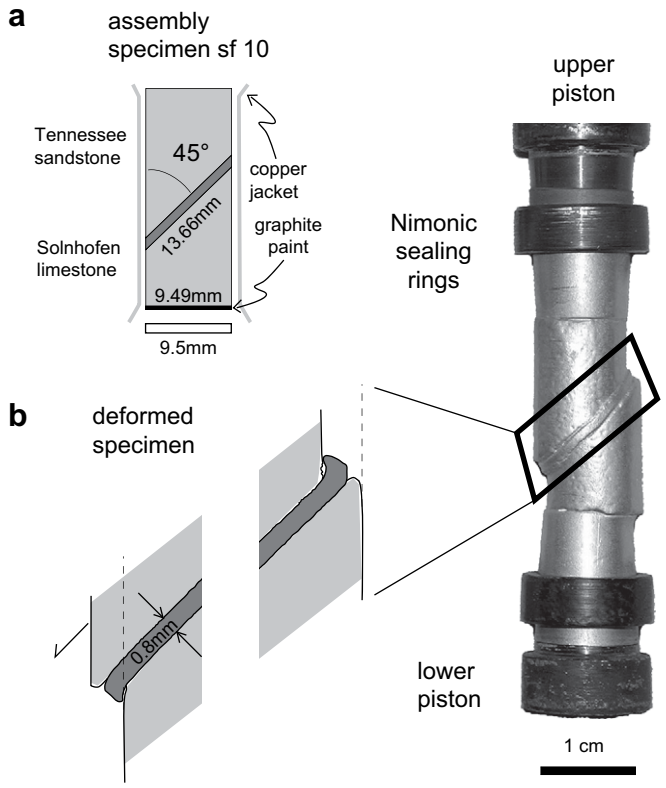

Fig. 1. Specimen assembly in direct shear (a) before and (b) after deformation.

shape fabric geometries in natural high-strain zones (e.g. Sanderson and Marchini, 1984; Robin and Cruden, 1994; Dewey et al., 1998; Schreurs and Colletta, 1998) although severe problems of compatibility of regional strains and displacements can arise from such an interpretation.

Except for deformation in the brittle regime (Dresen, 1991; Logan et al., 1992; Gu and Wong, 1994), little attention has previously been given to the development of strain heterogeneities within a single sample deformed using this arrangement and how they affect locally the microstructure, microfabric and the rheology. By using a fine-grained rock material, Solnhofen limestone, we have been able to observe development of strongly localized high-strain domains across the width of the specimen during high temperature plastic flow. These domains were defined on the basis of the microstructure using both optical and electron microscopy (electron back-scattered diffraction – EBSD), which allowed variations in the grain shape fabric and crystallographic preferred orientation patterns to be observed. We interpret their development in terms of strain hardening effects arising from the particular boundary conditions imposed by this experimental configuration, leading to the superposition of heterogeneous strain distributions, and discuss the implications of these results for deformation in natural shear zones.

2. Experimental approach

2.1. Starting material

The starting material, Solnhofen limestone, has been widely used in experimental deformation studies and has several advantages for this and a related previous study (Llana-Fúnez and Rutter, 2005). The average grain size is 4–5 μm, with rare larger grains dispersed throughout the rock. This allows local microstructural analysis to be made on a sufficiently large number of grains at key sites within heterogeneously deformed specimens, despite the requirement of the deformation apparatus to use small diameter specimens (~10 mm). The initial porosity of the rock is approximately 5% (Rutter, 1972) and it comprises more than 97 wt% calcite. Rare quartz grains (<0.1% volume) of *ca* 20 μm diameter are present as a secondary phase throughout the rock. Other impurities, mostly organic matter and clay minerals, occur along grain boundaries (Schmid et al., 1987). Such impurities in limestone act to impede calcite grain growth at high temperatures (Robinson, 1971; Walker et al., 1990; Rutter et al., 1994; Herwegh and Kunze, 2002). The grain size and its limited range, together with the low mobility of grain boundaries, leave this material able to deform plastically at the conditions given below without interference from other processes that might alter grain shape or crystallographic preferred orientation (CPO) (Schmid et al., 1987; Llana-Fúnez and Rutter, 2005).

In experimental studies prior to Llana-Fúnez and Rutter (2005), combined measurement of CPO patterns and their spatial distribution in heterogeneously deformed Solnhofen limestone samples were not possible. The grain size in Solnhofen limestone is too small to measure the complete CPO by optical microscopy and X-ray texture goniometry does not provide directly observable relationships between crystallographic and shape fabrics on a sufficiently small scale. X-ray texture goniometry requires a homogeneous fabric over a scale of several mm to obtain a meaningful CPO pattern. These limitations can now be circumvented by using EBSD techniques on selected areas within polished surfaces of deformed specimens (e.g. Prior et al., 1999).

2.2. Experimental procedure

Experiments were performed in a 'Nimonic' testing machine, so named for the Nimonic 105® nickel-based alloy (75% nickel and 25% molybdenum) from which the pressure vessel is fabricated. This alloy is mechanically strong and corrosion resistant to temperatures above 700 °C, so that it can be used with water as a hydraulic confining medium. The pressure vessel is heated externally and can operate leak-free for experiments of many weeks duration. Variation in specimen temperature parallel to the cylinder length was less than 3 °C. Axial load was measured with a semi-internal load cell with a stress resolution for the specimen diameter used of better than 1 MPa. Before assembly, specimens were pre-dried at 80 °C for several days, and were tested jacketed within 0.25 mm wall-thickness annealed copper sleeves. More detailed specifications of the testing machine can be found elsewhere (Walker et al., 1990; Covey-Crump, 1992).

Experiments were run at 600 °C, a confining pressure of 200 MPa and a constant displacement rate of 5×10^{-6} m s^{-1}, the latter implying a bulk shear strain rate of about 5×10^{-3} s^{-1} in the specimen geometry used. Bulk shear strains of up to 3 were attained. At these conditions, Solnhofen limestone deforms predominantly by intracrystalline plasticity, well within the dislocation creep (power-law creep) regime, where strain rate is proportional to stress to a power n of 4.7 (regime 2 in Figs. 2 and 14 of Schmid et al., 1977).

Slices of Solnhofen limestone between 2 and 1.5 mm thick were cut at 45° to the axis of cylindrical cores 9.5 mm in diameter, and the elliptical slices were ground down to wafers of between 1.8 and 0.9 mm (±0.1 mm) thickness (Table 1). Forcing blocks were fabricated from cylinders of 7% porosity Tennessee sandstone, cut at 45° to the cylinder axis. The elliptical surfaces were only ground, not polished, to preserve some roughness to inhibit slip against the limestone surfaces. The angle of the cut implies that the original bedding orientation in the limestone is always perpendicular to the bulk shortening direction in the sample assembly inside the testing machine. When assembled, the total length of the specimen assembly (sandstone and limestone) was approximately 20 mm

Table 1
Deformation tests on dry Solnhofen limestone at 200 MPa confining pressure and 600 °C

Test	Dimensional data		Bulk strain	
	Thickness, mm		Thinning, ε	Shear strain, γ
	Initial	Final		
Direct shear				
sf09	1.78	1.46	0.18	1.30
sf10	0.91	0.81	0.12[a]	2.66
sf24	1.46	1.30	0.11	0.76
sf25	1.42	1.19	0.16	1.39
Long cylinders				
sf16	19.37	15.03	0.22	–
sf37	21.09	15.53	0.26	–
sf38	22.23	15.07	0.32	–
Ten02	21.07	20.44	0.03	–
Short cylinders				
sf02	4.11	2.4	0.42	–
sf03	4.14	2.6	0.37	–
sf04	4.11	2.1	0.49	–
sf05	4.37	2.4	0.45	–
sf08	4.25	2.4	0.44	–
sf11	3.19	1.95	0.39	–

[a] Consistent with a finite change in length from 13.42 to 14.32 mm.

(Fig. 1). In addition to acting as forcing blocks, mimicking wall rocks in a fault/shear zone, the sandstone pieces also allowed venting of specimen pores to atmosphere *via* the hollow upper loading piston.

The base of the lower sandstone forcing block was painted with colloidal graphite paste to reduce friction and facilitate its lateral displacement (Fig. 1). This inhibits bending of the sample assembly, which would otherwise lead to an additional component of apparent strain hardening. Mechanical data were corrected for the elastic axial distortion of the machine plus sandstone forcing blocks and for the load supported by the copper jacket (Fig. 2). The jacket strain hardens considerably, supporting an apparent shear stress of up to 10 MPa (about 5% of the total stress supported) by a shear strain of *ca* 3 (Mariani, 2002).

As shearing occurs in a vanishingly thin specimen, the effective area of the specimen supporting the load becomes smaller as the two elliptical surfaces are displaced against each other. The effective area is the projection of one ellipse into the other following the direction of the loading axis. In this case a correction would have to be applied for the effective area change in the calculation of shear stress. If the specimen used is thicker, it is to be expected that the area correction will become smaller, because axial stress

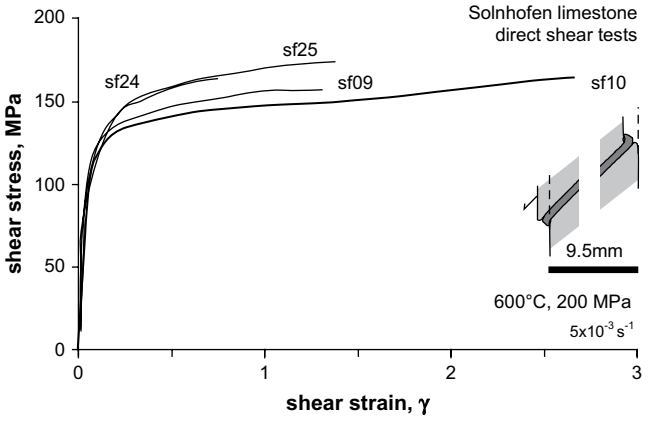

Fig. 2. Shear stress versus. shear strain curves in direct shear experiments. Test numbers correspond to those in Table 1.

trajectories will refract across the specimen layer, so that load is supported even by that part of the specimen displaced beyond the overlapping ends of the forcing blocks, provided the deformed ends of the specimen do not detach from the forcing blocks. Stress refraction is required because the outer surface of the jacketed specimen assembly must be parallel to principal stress trajectories owing to the zero shear stress boundary condition imposed by the hydrostatically pressurized confining medium. Even apart from this contributing factor, elastic contrasts between the specimen and forcing blocks, and the progressive development of CPO in the specimen cause stress refraction effects at the interface (Casey, 1980; Dresen, 1991; Gu and Wong, 1994). Shimamoto and Logan (1981) and Post and Tullis (1999), for example, deforming finite thickness specimens in direct shear, did not apply any apparent area reduction correction with progressive shear displacement at all. Given the complexity of attempting to resolve this issue from a theoretical point of view, we deformed prismatic specimens of metallic lead (0.9 and 3.2 mm thicknesses, and 1.5 and 3.0 mm length in the shear direction) to shear strains ~3 all at the same shear strain rate. Within experimental uncertainty these tests showed that with progressive shear, load continues to be transmitted across the almost full initial area of the specimen. We have therefore not applied any area correction to our direct shear data.

An additional set of standard axisymmetric shortening tests on long cylinders of Tennessee sandstone and Solnhofen limestone was carried out to establish that at the experimental conditions the sandstone is much stronger than the limestone at the imposed pressure/temperature conditions, and hence that all measured deformation occurred only in the limestone slices. These experimental data were corrected for cross-sectional area increase with shortening in the conventional way that assumes homogeneous deformation at constant volume. We will also make reference to our earlier experimental data (Llana-Fúnez and Rutter, 2005) on the axisymmetric compression of thin discs of Solnhofen limestone to help to evaluate the influence of the component of flattening normal to the sheared limestone slab that inevitably occurs with this specimen geometry and which causes deviation from what would otherwise be a simple shear deformation geometry.

2.3. Microstructural analysis

Microstructural observations were made on the profile section parallel to the axis of symmetry of the cylinder and perpendicular to the slice of limestone, through the central part of the specimen slice (Fig. 1). The sections were cut parallel to the transport direction of one forcing block with respect to the other, equivalent to the 'tectonic transport direction' in naturally deformed rocks. Deformed specimens were prepared as polished blocks to a surface finish of 0.05 μm gamma-alumina. EBSD analysis required further Syton®-polishing. EBSD patterns were collected automatically using a step size of 1 μm, slightly smaller than the starting grain size, to allow adequate mapping of CPO in calcite both in high- and low-strain areas. Rates of successful identification of crystal orientation by the CHANNEL® software were in general on the order of 50% for most EBSD maps (rates depend on pattern quality, in most cases in relation to surface quality).

The grain shape fabric in micrographs was observed using reflected light in a conventional optical microscope (e.g. Bestmann et al., 2000; Llana-Fúnez and Rutter, 2005).

3. Experimental results

3.1. Stress/strain behaviour

Test conditions and mechanical data for all tests reported are given in Table 1. For the direct shear tests, plots of shear stress

versus bulk apparent shear strain resolved parallel to the plane of the specimen are shown in Fig. 2 and show reasonable reproducibility of general mechanical behaviour. Apparent variability in strength between different tests (Fig. 2) appears to be attributable to differences in the starting thickness of the limestone specimens (see Table 1), which results in different amounts of thinning of the specimen normal to the slice thickness. Limited slip along the limestone–sandstone interface did occur in some experiments, but with no significant effect on strength, making it difficult to establish the exact strain accumulated in those specimens, which are not reported here. More commonly, the rupture of the copper jacket (in six other experiments not all reported in Table 1) that isolates the specimen from the confining medium resulted in brittle failure by the sudden reduction of effective pressure.

The block of Solnhofen limestone from where the specimen cores were obtained shows yielding to permanent strain at similar stresses to those reported previously (Schmid et al., 1987). Beyond the yield point, all stress/strain curves show substantial strain hardening.

Stress/strain curves for several conventional axisymmetric shortening experiments on 20 mm long cylinders of Solnhofen limestone compressed normal to bedding at 600 °C and 200 MPa confining pressure are shown in Fig. 3 for comparison with the stress/strain behaviour of Tennessee sandstone. The limestone deformed plastically with a small initial amount of strain hardening from a yield stress of 210 MPa, whereas the sandstone continues to deform elastically to stresses above 500 MPa. Failure of the sandstone forcing blocks is therefore not expected to contribute to apparent strain in the direct shear experiments.

Fig. 3 and Table 1 also show stress/strain data for short cylinders (initially nominally 4 mm long) deformed at the same temperature and pressure and the same initial strain rate. These data are presented using a function for cross-sectional area correction that corresponds closely to the assumption of homogenous strain at constant volume at small strains (<15%) but which becomes smaller at higher strains, when the outermost extruded part of the specimen supports progressively smaller fractions of the total load. These specimens are characterized by a higher yield stress than the long cylinders, followed by a longer period of strain hardening. The flow stresses and apparent hardening rates at strains above about 25% shortening are not considered very reliable. The hardening observed at low to intermediate strains is considered attributable to the effects of heterogeneous deformation and strain rate hardening. The average instantaneous strain rate alone increases almost twofold during the experiment as the specimen thins, hence stress increases according to the material rheology. The heterogeneous deformation that occurs results in even greater local strain and strain rate variations.

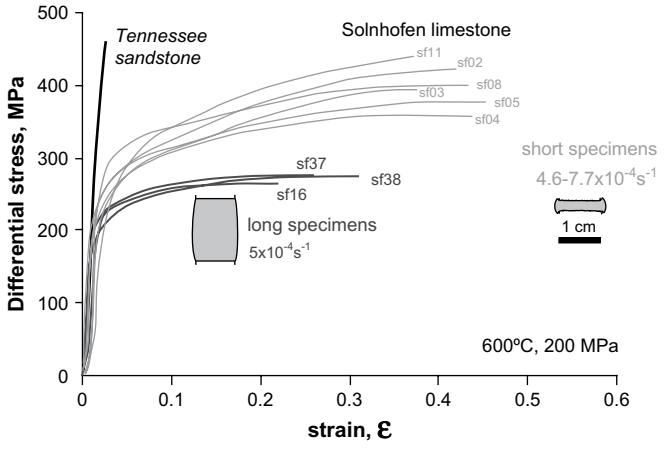

Fig. 3. Differential stress versus strain curves for axisymmetric shortening tests at 600 °C, 200 MPa confining pressure (a) on long cylinders of Solnhofen limestone and one test on Tennessee sandstone (terminated whilst still in the elastic region before failure), and (b) on short cylinders of Solnhofen limestone (data from Llana-Fúnez and Rutter, 2005). Test numbers correspond to those in Table 1.

3.2. Shape fabric in calcite

During loading, the asperities in the sandstone intrude into the limestone so that the open pore space at the sandstone surfaces becomes filled with plastically intruded asperities of limestone, helping to inhibit slip. During progressive deformation, the calcite grains developed a shape fabric, observed on the shear-parallel profile section of the specimen (Fig. 4). In every deformed sample this fabric was seen to be continuous from each of the contacts with the sandstone towards the middle of the limestone slice and has a sigmoidal trace (Fig. 4a). The shape fabric varies in intensity, from very intense close to the sandstone blocks (grains showing aspect ratios over 10:1, see Fig. 4b) to very weak or barely recognizable in the middle of the specimen (Fig. 4c). Thus these tests characteristically developed two localized shear bands symmetrically disposed about the centre line of the limestone slice. Tests carried out to increasing bulk shear strains in different samples indicated that the high-strain bands nucleated almost at the edge of the boundary asperities and widened with progressive strain towards the centre of the limestone slice with increasing bulk strain.

A map of the shape fabric, made by hand drawing the orientation of the calcite grains in a mosaic of micrographs covering a whole specimen (sf10), shows that the sigmoidal shape of the foliation is present everywhere with the exception of the edges of the limestone slice where sample extrusion and limited injection of copper along the sandstone/limestone interface occurred (Fig. 5).

From the centre of the specimen towards the planar edges there is initially a continuous increase in the apparent aspect ratio of calcite grains. Grain boundaries are initially sharply defined and relatively straight. Calcite grains that were stretched to an aspect ratio of ~10:1 have grain boundaries that developed a wavy appearance, showing a regularly spaced pinch-and-swell profile to the point of isolating new, smaller grains (Fig. 4b). The width of stretched grains in the profile section examined, around 1 μm, also corresponds to the spacing of the pinch-and-swell and the size of the resulting new grains. The elongated grains also show undulose extinction that makes it harder to identify individual grains clearly.

3.3. Crystallographic preferred orientation (CPO)

Crystallographic preferred orientation patterns produced in direct shear are presented both as pole figures of crystallographic axes and planes as well as inverse pole figures (IPFs) (Fig. 6). The crystallographic elements used correspond to slip directions and slip planes of major slip system families in calcite at relative high temperatures: $c\langle 11\bar{2}0\rangle$, $r\{10\bar{1}4\}\langle 02\bar{2}1\rangle$ and $f\{01\bar{1}2\}\langle 10\bar{1}1\rangle$ (based on De Bresser and Spiers, 1997). For the description of pole figures of various crystallographic elements two reference frames will be used: the structural reference frame (X_i, Y_i, Z_i) refers to the orientation of local shape fabric and the experimental reference frame (X_0, Y_0, Z_0) refers to the orientation of the sandstone–limestone interface, which coincides with the general bulk shear plane, its normal and the 'tectonic transport direction'. The latter is also the reference frame used in the EBSD pole figures. IPFs were constructed for each of three orthogonal directions, nominally parallel to the local extension and shortening directions, and normal to the other two, i.e. perpendicular to the plane of measured section. The first two directions are almost parallel to the orientation of the shape fabric (the departure from parallelism increases with non-coaxiality of the strain).

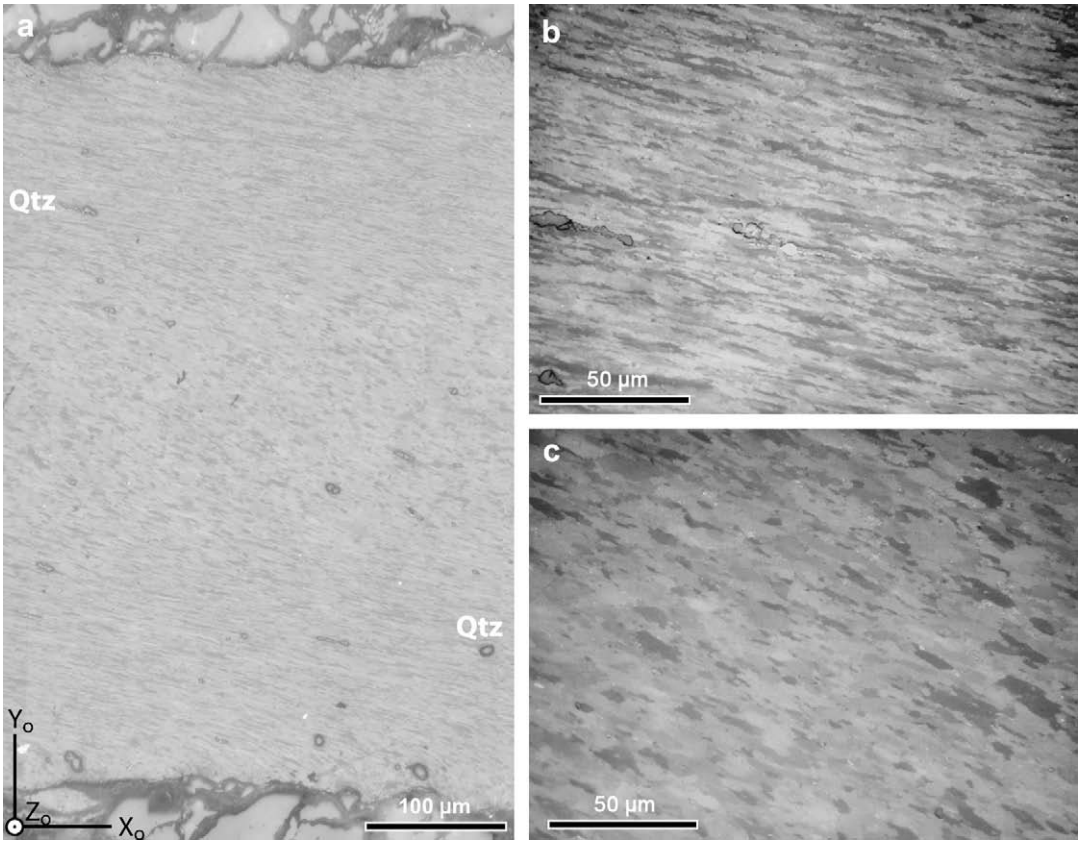

Fig. 4. Reflected-light micrographs taken from a traverse across deformed specimen sf10 from the upper to lower sandstone forcing block in the central part of the sample. (a) Shows the shape fabric in calcite (left-lateral shear sense). The few grains with higher relief within the limestone are isolated grains of quartz. (b) Higher magnification image from one of the high-strain bands. (c) Detail of the low-strain area in the middle of the specimen. (b) and (c) have the same magnification and orientation.

The initial calcite CPO in Solnhofen limestone in the block we used is characterized by a broad girdle of *c*-axes parallel to the bedding plane with a maximum intensity of 1.9 times uniform distribution (Llana-Fúnez and Rutter, 2005), which is modified by the deformation imposed upon the specimen.

In the sheared specimens, CPO patterns in the low finite strain domain differ from patterns in the high-strain bands. *c*-Axes in the low-strain domain either concentrate in a broad great-circle girdle parallel to the shape fabric or define incomplete double or cleft minor-circle girdles, centered around the local extension direction (map m1 in Fig. 6). The *c*-axis girdles are symmetric with respect to the structural reference frame (the shape fabric), and have no clear internal asymmetry (corresponding to difference in density or intensity of *c*-axis preferred orientation from left to right or from top to bottom of the upper hemisphere shown; see Passchier and Trouw, 1996). The preferred orientation of known calcite slip directions $a\langle 11\bar{2}0\rangle$, $\langle 02\bar{2}1\rangle$ and $\langle 10\bar{1}1\rangle$ (corresponding to slip planes *c*, *r* and *f*, respectively) display an asymmetric arrangement with respect to both the structural and the experimental reference frames, the girdles are slightly rotated with the sense of shear. Direction $\langle 02\bar{2}1\rangle$ shows a maximum $\sim 10^\circ$ off the limestone–sandstone interface and double or two minor cleft circle girdles centered on it. Slip planes $r\{10\bar{1}4\}$ and $f\{01\bar{1}2\}$ mimic slightly the crystallographic pattern of the *c*-axis but with a reduced intensity (Fig. 6a). The directions parallel and perpendicular to the shape fabric (X_1 and Y_1) show characteristic orientation patterns in inverse pole figures corresponding to clear extension and shortening directions (see Rutter et al., 1994; Llana-Fúnez and Rutter, 2005). The third direction, Z_0 (=Z_1), normal to the plane of observation, resembles an extension direction but it is not well developed.

Towards the high-strain domains, the tendency in the *c*-axis fabric is to strengthen the double cleft girdles and to reduce the

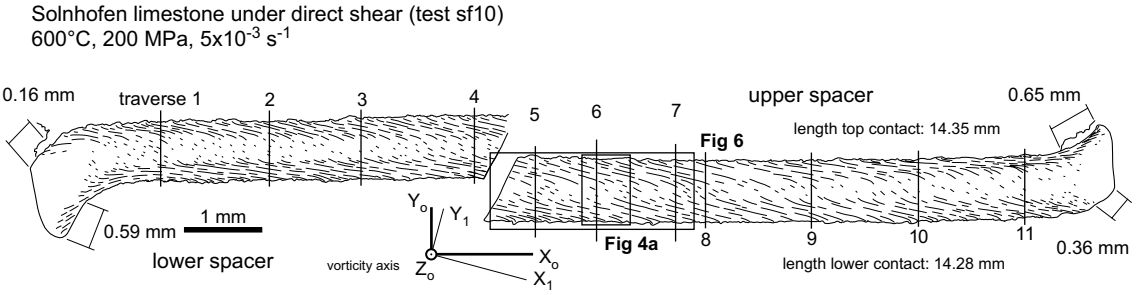

Fig. 5. Manual tracing of the shape fabric in calcite grains across the central part of deformed specimen sf10 from a micrograph collage. A series of numbered lines indicate the location of traverses where shape fabric long axis angles were measured for Fig. 9. Also indicated are the locations of the areas used for EBSD analysis and the location of the micrograph in Fig. 4a. Lengths of the extruded ends of the specimen are indicated in mm.

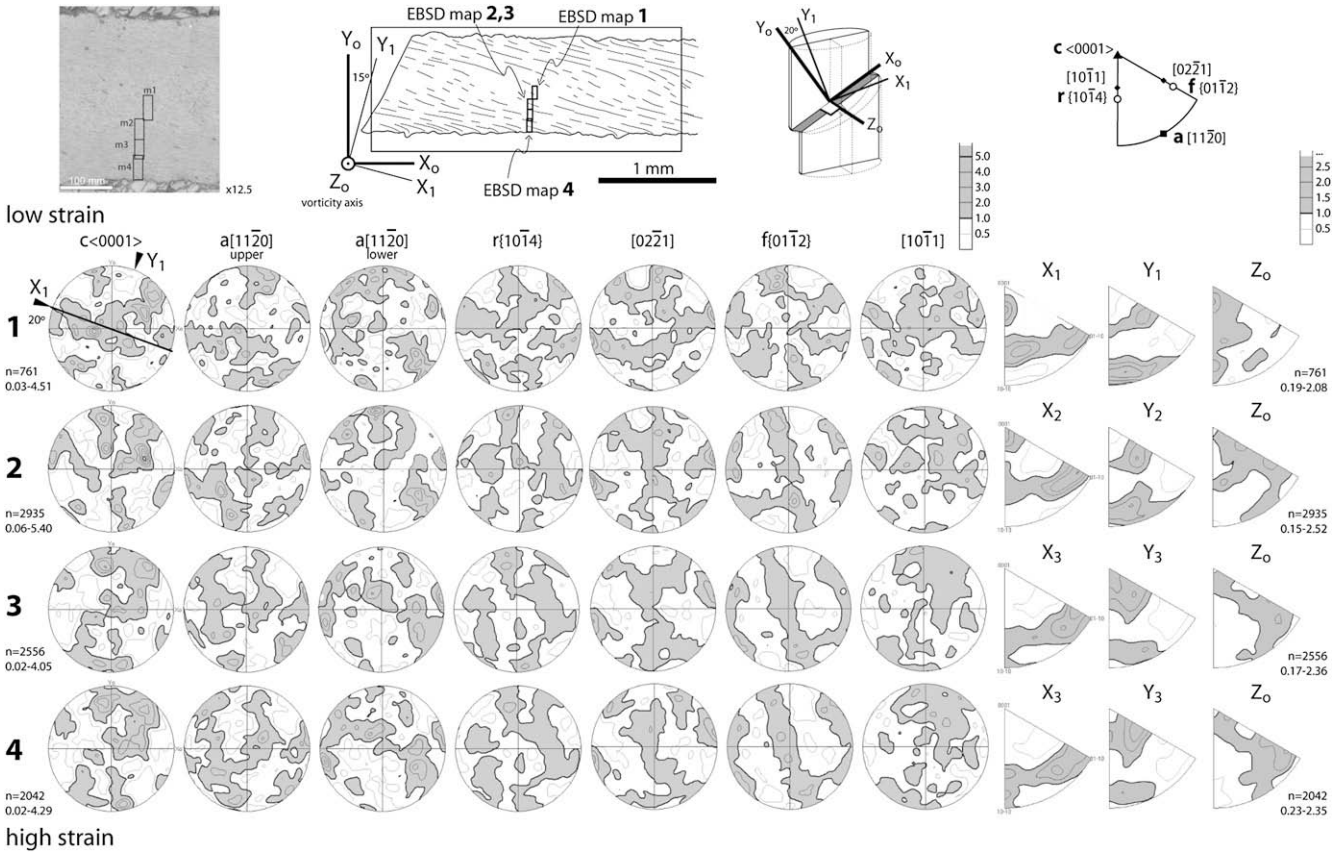

Fig. 6. Upper hemisphere stereoprojections showing crystallographic preferred orientation (CPO) patterns in three contiguous EBSD maps, both located as per the top left micrograph and upper shape fabric map. The middle map has been split into two maps of similar size (m2 and m3) to the neighbouring maps (m1 and m4). Contoured pole figures (contour spacings are indicated in the top right corner as multiples of a uniform distribution) of the main three slip system families in calcite at high temperature conditions (based on De Bresser and Spiers, 1997) are shown: $c(0001)\langle 11\bar{2}0\rangle$ ($c\langle a\rangle$), $r\{10\bar{1}4\}\langle 02\bar{2}1\rangle$ and $f\{01\bar{1}2\}\langle 10\bar{1}1\rangle$. To the right are inverse pole figures corresponding to local shortening and extension directions in the pole figures. CHANNEL 5® software was used for contouring.

great-circle girdle component parallel to the foliation to a single maximum following the stretching direction (which almost disappears in the highest strain domain, m3). All slip directions $a\langle 11\bar{2}0\rangle$, $\langle 02\bar{2}1\rangle$ and $\langle 10\bar{1}1\rangle$, show an asymmetry with a rotation axis parallel to Z_0, following the externally imposed sense of shear. *a*-Axes are arranged in poorly developed double small-circle girdles and in one stronger maximum. All are oblique synthetically with the sense of shear to the shape fabric. Slip direction $\langle 02\bar{2}1\rangle$ defines a strong maximum (rotated with the sense of shear) and a crossed girdle, which is not only rotated but has an internal asymmetry with one long arm being almost straight and the other showing two kinks. The kinks, located at $\sim 45^\circ$ at either side of the bulk shear plane (normal to Z_0) show similar pattern to main slip directions in quartz at high temperature, i.e. *c*-axis (see Schmid and Casey, 1986). CPO patterns in relation to $f\{01\bar{1}2\}\langle 10\bar{1}1\rangle$ are poorly developed.

Planes $r\{10\bar{1}4\}$ and $f\{01\bar{1}2\}$ define minor and great-circle girdles that centre around the main slip direction in $\langle 02\bar{2}1\rangle$ and are symmetric with respect to it. In inverse pole figures, the orientation patterns of the directions parallel and perpendicular to the shape fabric are also typical examples of extension and shortening directions. The *Z* direction is not well developed in either EBSD map 2 or in map 3 (Fig. 6).

4. Analysis of strain

4.1. Bulk strain

The specimen sf10 was initially the thinnest slice of Solnhofen limestone tested and hence reached the highest bulk strain of all direct shear experiments run successfully (Table 1). The existence of measurable thinning of the limestone slice in direct shear tests implies that the experimental deformation was not strictly in plane strain conditions. In specimen sf10, bulk finite thinning measured is about 12%. This is consistent with the lengthening of the specimen along the profile section, which was estimated from Fig. 5 to be 6.7%, the reminder of the thinning being compensated by lateral extrusion normal to the plane of observations.

Finite strain associated with the shape fabric can therefore be considered to comprise two components that probably developed simultaneously: a coaxial (irrotational) component related to the thinning of the limestone slice, and a non-coaxial (rotational) component related to the shear produced by the relative lateral movement of the forcing blocks (Fig. 7). The observed grain shape variations imply variations of up to $\times 10$ in the amount of strain within and without the localized shear zones. These two strain components are considered below.

4.2. Orthogonal thinning strain component

From the orientation of the finite shape fabric alone it is not possible to determine the relative contributions of both shear and flattening components at any one part of the traverse across the width of the specimen. It is, however, helpful to make certain inferences about the nature of the contribution of the less dominant component overall, which is the thinning component. There are two possibilities; the first would be to assume that shortening is homogeneous across the specimen slice, and the second that it is heterogeneous (by analogy to numerical modeling of transpression

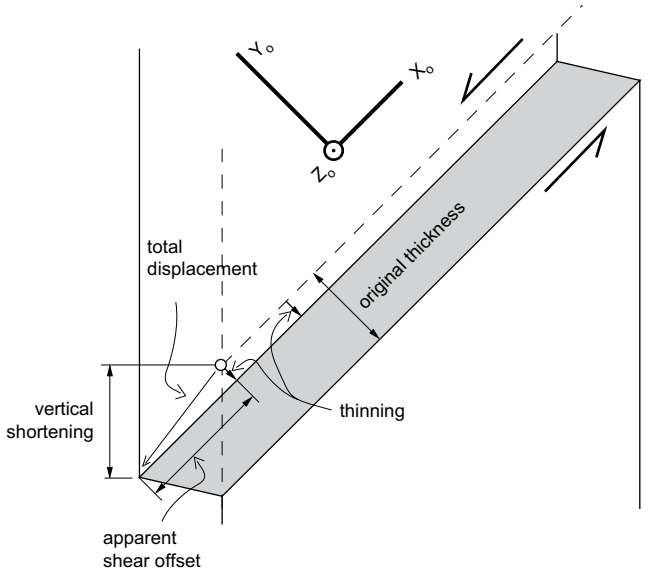

Fig. 7. Geometry of direct shear experiment using saw cut spacers at 45° to show the relationship between shear and flattening displacements. Known initial and final lengths are indicated.

in shear zones, Robin and Cruden, 1994). The observed lack of slip along the limestone–sandstone interface rules out homogeneous shortening completely. Thinning strain ε_{Y_0} must be zero at the interface and may reach a maximum in the middle of the specimen. To characterize the gradient of the thinning (and concomitant lateral extension) across the limestone slice, we used as a proxy the extrusion profiles obtained from axisymmetric compression tests on short cylinders of Solnhofen limestone, deformed at similar conditions (Llana-Fúnez and Rutter, 2005). Based on the latter study, and having measured the initial and final thicknesses of the specimen slices, the simplest assumption we can make is that the distribution of radial extensional strain will be the same in the direct shear tests, and also that it would be isotropic in this plane. In this way we have made a best-estimate of the distribution of strain ε_{Y_0} across the slice (Fig. 8). Fig. 8b shows that in the case of the direct shear tests, the maximum shortening strain in the middle of the specimen would have reached almost 20%, decreasing progressively to zero at both interfaces with the forcing blocks.

4.3. Rotational strain component

The angle of the shape fabric in the calcite rock with respect to the limestone–sandstone interface was measured in specimen sf10 in a series of traverses across the deformed slice (Fig. 5). It did not prove feasible systematically to measure grain axial ratios owing to the development of undulating and pinched grain boundaries in the more highly strained grains. If the deformation were only by simple shear the grain long axis orientation could be related directly to distortional strain. In these experiments the deformation is demonstrably more complex than this, on account of the superimposed thinning strain. However, it is qualitatively clear (Fig. 5) that the more rotated grain long axes tend to belong to the more highly strained grains, therefore we can use grain long axis orientation as a qualitative index of the amount of distortional strain by shearing.

The orientation of the long axes of the calcite grains in all these traverses is shown in Fig. 9. A polynomial fit of fourth degree was applied to the raw data to describe quantitatively the variation in orientation. The maximum angle of the shape fabric with respect to the sandstone–limestone interface is 35–40° decreasing to about

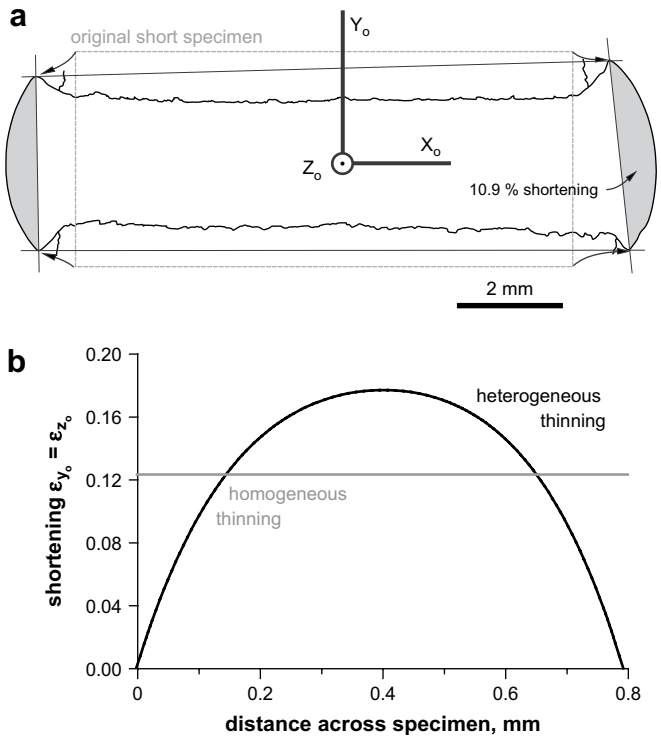

Fig. 8. (a) Profile section of a short specimen of Solnhofen limestone deformed dry at 600 °C and 200 MPa confining pressure in axisymmetric compression (Llana-Fúnez and Rutter, 2005), used as a reference to estimate the thinning gradient across the specimen in direct shear tests. (b) Shows the adopted strain profile taken to correspond to direct shear test sf10 as shortening versus distance across the deformed specimen.

10–15° in the high-strain areas. There is a marked angular maximum in the central section of the specimen, where the long axis angle is $30 \pm 5°$.

The pattern of development of orientation of strain ellipsoid long axes and finite strain ellipsoid shape when two homogeneous strain fields are superimposed depends on the order of superimposition, and the situation becomes more complex still when the superimposed strain fields are heterogeneous (Ramsay and Huber, 1983). For example, a given amount of simple shear followed by a given

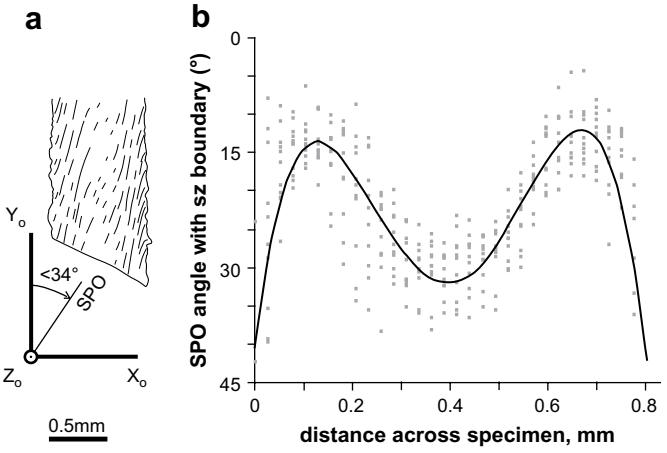

Fig. 9. Orientation distribution of the long axis of the shape preferred orientation of calcite grains measured in traverses (locations in Fig. 5) plotted with respect to the distance across specimen sf10. A polynomial fit of 4th fourth degree was applied to describe quantitatively the variation in angle and also to smooth the data.

amount of flattening normal to the shear plane produces a finite strain ellipsoid whose shape is more flattened and whose long axis is more rotated towards the shear direction than when the flattening is applied first followed by the shearing. When a heterogeneous flattening of the type expected in these Solnhofen limestone slices is combined with homogeneous simple shear, irrespective of the order of imposition of the strains, a single sigmoidal shear zone should be produced in the centre of the slice, with maximum finite strain and maximum rotation of the ellipsoid long axis towards the shear direction in the middle of the slice. The order of imposition of the strains only affects the details of the shapes and orientations of the long axes, not the overall pattern expected, but these considerations mean that we cannot separate the progressive simple shear components from the heterogeneous flattening components by means of analysis of the finite shapes of grains. Further complexity arises from the need to consider the compatibility of the layer-parallel extensional strains across the width of the layer. On the other hand, because the overall amount of thinning of the slice and the apparent total shear offset are known from direct measurements (Fig. 7), we can deduce these to be, respectively, a bulk thinning of 12% and a bulk shear strain, γ, of 2.7 in specimen sf10, for example.

The occurrence of a strain minimum in the central region of the limestone slice, rather than a maximum that might be expected, suggests that the strain heterogeneity arises from rheological inhomogeneity, i.e. the low finite strain tract is stronger than the tracts on either side, so that only smaller shear strains can accumulate there.

4.4. Distribution of strain and relation to CPO

The geometry of the orientation distribution of the long axes of grains and the correlation with degree of grain flattening allow two planar domains of high-shear strain to be defined in a typical specimen, with a central zone of lower shear strain in which thinning strain is expected to be maximized, by analogy with the results reported by Llana-Fúnez and Rutter (2005). This arrangement of coaxial and non-coaxial strain and the progressive switch in deformation geometry is also reflected in the geometry of CPO patterns (Fig. 6). In map 1, located in the middle of the specimen, *c*-axes show a pattern characterized by a great-circle girdle following approximately the shape fabric and two small-circle girdles centered on the location of the local shortening direction. This geometry resembles the CPO patterns in Solnhofen limestone undergoing flattening in axisymmetric shortening experiments (Llana-Fúnez and Rutter, 2005). Towards the high-strain bands (map 4), there is a progressive disappearance of the single great-circle girdle centered on the compression axis and a strengthening of double small-circle girdles (cleft girdles) centered on the local extension direction X_1. There is an additional increase in the asymmetry of ⟨0221⟩ direction patterns (corresponding to predominant slip direction along *r* planes) in maps 2 and 3 (where shear strain is highest). The development of cleft girdles around the extension direction and the increase of asymmetry suggest a predominant role of the extension direction in non-coaxial deformation, matching what is inferred from the analysis of the shape fabric.

5. Evolution of strain and rheological behaviour

In a material of simple rheology, deformation occurs at constant stress, constant strain rate and constant temperature, and the rheological properties do not evolve with strain. However, Solnhofen limestone at 600 °C displays significant strain hardening. Fig. 3 shows stress/strain curves for short cylinders of Solnhofen limestone (from Llana-Fúnez and Rutter, 2005). During 50% shortening, apparent strength increases almost twofold and is particularly rapid in the early post-yield stages. Even long cylinders show substantial rates of strain hardening (Fig. 3) during the first 10% of strain. Short cylinders show apparent hardening not only due to CPO development and the evolution of dislocation substructure, but also due to the twofold increase in strain rate that accompanies shortening at constant bulk displacement rate and the marked heterogeneity of the flow that is forced by the geometry of the thin specimen (Fig. 8). At 600 °C, Solnhofen limestone is also characterized by a very non-linear stress/strain rate relationship (power-law with a stress exponent of *ca* 5, Schmid et al., 1987). This means that small changes in stress (at a given strain) produce large changes in strain rate. We therefore suggest that the development of two separate shear zones separated by a zone of low shear strain in these experiments can be explained through the effects of the heterogeneous strain on rheology through strain and strain rate hardening.

Fig. 10 shows qualitatively that in the central part of the specimen, owing to its inhomogeneity, the flattening strain may be commensurate with the rotational shear component, whereas towards the edges the shearing strain dominates. The hardening associated with the higher thinning strain in the centre likely inhibited the development of shear strain in that region, forcing the shear strain to localize closer to the forcing blocks into two separate bands. The most extreme manifestation of such an effect would be if the flattening strain were imposed first, producing maximum strength variation across the thickness of the slice, followed by the shearing displacements. In reality, increments of flattening and shearing probably proceed together. The ways in which strain is partitioned into the shear zones and into producing the flattening profile will then be sensitive to the relative rates of hardening produced in the two flow modes, but comparing Figs. 2 and 3 implies that the flattening strain produces more rapid hardening. This will be influenced further by the progressive development of plastic anisotropy through the formation of different CPOs, but this will additionally complicate the strain evolution by permitting

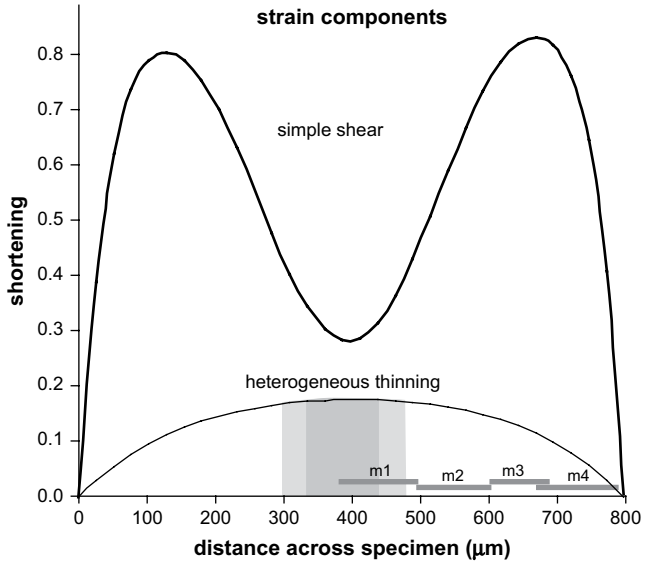

Fig. 10. Indication of the relative contributions of the two strain components in specimen sf10, expressed as the maximum shortening strain for the finite strain ellipse. Coaxial strain corresponding to heterogeneous thinning of the specimen is based on the profile in Fig. 8. Non-coaxial strain is based on the deflection of the shape fabric shown in Fig. 9 with respect to the specimen boundary, assuming simple shear and correcting for lengthening and shortening of the specimen associated to the bulk thinning. Approximate location of EBSD maps in Fig. 6 are is indicated at the base of the graph (m1 through –m4). Despite the semi-quantitative nature of this figure, it indicates that in the centre of the specimen (grey shading), the relative contributions of strain due to heterogeneous thinning and shear may be similar.

stress refraction, so that local strain rate variations will develop depending both on hardening evolution and development of local variations in stress intensity. That hardening also progressively develops in the areas dominated by rotational strain is testified by the observed tendency for the strongly sheared bands to widen towards the centre of the specimen as shear displacement increases.

To illustrate the development of paired shear zones in a strain hardening material approximating to Solnhofen limestone we carried out a simple numerical simulation of incremental shear parallel to the layer with intercalated increments of flattening strain normal to the layer, corresponding to the situation in the central part of the specimen from which the measurements for Fig. 5 were made. The result is shown in Fig. 11. The layer was divided into 20 slices of equal thickness. The rate of thinning in each slice was made to vary linearly, from zero at the margins of the layer to a maximum in the centre, such that overall thinning during the shearing was 10%, to correspond to specimen sf10, with a maximum thinning in the central slices of 17%. Based on strain hardening data for the compression of thin cylinders of Solnhofen limestone (Fig. 3), this causes almost twofold strain hardening relative to the yield stress. Total shear displacement for the layer was divided into 25 increments, with small shear and flattening increments being applied alternately. The reduction of shear strain rate with incremental hardening caused by the flattening strain was calculated assuming a power-law rheology with a stress exponent of 5. A total bulk shear strain of 1.83 was applied (broadly comparable to specimen sf10), and this led to a maximum shear strain in the outermost layers of 3.9. For simplicity, no allowance was made for compatibility of extensional strains between the layers. This means that the layers are not mechanically coupled. However, because the flattening is axisymmetric in the central part of the specimen, the difference in layer-parallel extensional strain between layers is less than 1%. Therefore this assumption is not expected to have a marked effect on the local strain magnitudes and orientations.

The computed strain pattern (Fig. 11) reproduces quite well the main features of the experimentally produced pattern (Figs. 4 and 5), in terms of the orientations of the principal strains and their magnitudes, and supports the interpretation proposed above to explain the formation of paired shear bands. The local reduction in shear strain immediately adjacent to the forcing blocks is not reproduced, however. We suspect that in the experiments this arises from local hardening effects associated with the irregular form of the surfaces of the forcing blocks at the grain scale (Fig. 4a) and the requirement for the outermost calcite grains to deform to infill the surficial irregularities when confining pressure is applied. Also, the model predicts a rotation of the principal strains in the centre of the slice towards normality and parallelism with the length of the slice, as the thinning strains dominate in the middle. This should cause a small local increase in the shape preferred orientation (SPO) angle on Fig. 9 in the centre of the slice, superimposed on the minimum observed. Such an increase is not resolved on the data, perhaps because of the angular spread of the data coupled with the difficulty of sketching the grain long axes when the local grain shape aspect ratio is close to unity.

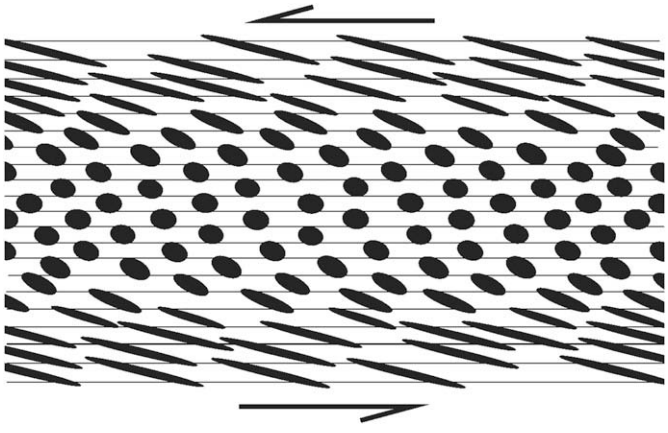

Fig. 11. Simulation of the production of paired shear bands as a result of strain hardening arising from coaxial flattening strain normal to the specimen slice being greatest in the middle zone of the specimen. Ellipses show the orientation and magnitude of local strains. The specimen is divided into 20 parallel slices, each originally the same thickness. Total thinning of the layer is 10% and bulk shear strain = 1.83. Maximum shear strain = 3.9. The middle layers are thinned by 17%, resulting in local strain hardening by ×x2, in approximate correspondence with data shown in Fig. 3. Strain rate reduction in the middle layers corresponds to a power- law rheology with stress exponent of 5.

6. Relevance of direct shear experiments for natural deformation

Unlike the torsion test, the direct shear test as used in triaxial testing machines has stress boundary conditions. Before load is applied, there is no difference in stress between the hydraulic confining pressure applied radially to the elliptical specimen and the stress normal to the plane of the specimen. As differential load is applied, the stress normal to the specimen plane increases in proportion to the shear stress resolved along the plane of the sample. The limited lateral extent of the specimen allows material to be extruded laterally. In nature, the classical shear zone is inferred to have (a) undeformed wall rocks and (b) a large lateral extent in the plane of the shear zone relative to its thickness, so that lateral extrusion is prevented. These conditions mean that simple shear alone, or simple shear plus shortening normal to the shear zone accompanied by compensating volume loss are the only possible strain pathways (Ramsay and Graham, 1970).

It seems likely that only in special circumstances will geological situations arise in nature that are directly comparable to the experiments described here, and which might by implication give rise to comparable structures. The main requirement is the presence of a region where "sheared" rock can be extruded to. A possible scenario might arise at great depth in a migmatite complex, where the conditions of laterally infinite extent of a shear zone may be relaxed where partially molten regions bearing shear zones are bounded laterally by melt bodies. The evolution of hardness within a shear zone can in such circumstances be determined by movements and segregations that cause variations in melt fraction and hence strength.

Another scenario is that of crustal transpression zones. That is, subvertical or inclined strike-slip faults and/or shear zones, where the shear zone core may be extruded vertically or towards the foreland (Sanderson and Marchini, 1984; Robin and Cruden, 1994; Jones et al., 1997; Dewey et al., 1998). Compare also the kind of scenario envisaged for mid-crustal extrusion in the Himalayan orogen (Beaumont et al., 2002). Dewey et al. (1998) show that different patterns of superposition of flattening and shear strain, and hence different fabric patterns can develop in transpression zones, according to how strains are superimposed, with fabric patterns varying not only across a transpression zone but also along it, as the amount of extrusion-associated transport varies. One of their suggested fabric patterns (their Fig. 6c) is very similar in form to that which we report here, although Dewey et al. (1998) consider only finite strain superpositions and not how they may be influenced by evolving rheological behaviour. In the context of strain variation along a transpression zone, it should be noted that the observations we describe were made in the centre of the specimen slice, from where the extrusion flow diverges and hence where the

flattening strain remains closest to irrotational (e.g. Llana-Fúnez and Rutter, 2005). On either side of the point of flow divergence, progressively greater shearing strains develop by viscous drag adjacent to the margins of the specimen slice. Hence the detailed pattern of strain superimposition should vary along the edge of the specimen, differently in either direction away from the divergence point because in one direction the boundary-parallel shear strains are co-operative whilst in the opposite direction they are counteractive. We have presently not attempted to study such variations. These effects are not immediately apparent in the observed fabric orientation patterns (Fig. 6), perhaps because in these experiments flattening strains are dominated by the much larger superimposed shear strain components.

A commonly observed pattern of heterogeneous strain in nature is in a multilayer in which schistosity refracts between layers of contrasting amounts of deformation. These have been studied from the theoretical point of view (Treagus, 1981, 1988, 1993) and also experimentally using analogue models (Treagus and Sokoutis, 1992). In these models, strain localization is related to stress amplification generated due to the boundary conditions and the difference in effective viscosity, or competence contrast, between competent sandstone and incompetent shale layers (viscosity ratios up to 62 times). The scale and range of the stress amplification in high-stress areas to be expected depend on the rheology of the weak layer, its thickness and the mechanical contrast with the stiffer layers. In these models, linear and power-law rheologies were assumed for adjacent layers, with material properties remaining constant with time and/or strain. Similar structural features developed as in our experiments, although in our case the effective development of rheological layering is attributable to strain dependence of the rheology coupled with substantial non-linearity, rather than to lithologic contrasts or effects arising from metamorphic or chemical changes.

Finally, paired high-strain shear zones have recently been described on either side of aplite dykes intruded into granodiorites in the European Alps by Mancktelow and Pennacchioni (2005). Coaxial low-strain concentrates in the granodiorites, that only develop shows substantial shearing in the vicinity of the contact with stronger aplite dykes or alteration haloes around veins. Note that the relative arrangement of strong versus weak materials is opposite to that in our experiments. The stronger and stiffer rock, the aplite, has a tabular shape and it is embedded in the more deformable granodiorite. Elastic properties for both materials (aplite and granodiorite) are similar, since late fracturing cuts across the aplite–granodiorite contact without deviation. It is only under amphibolite facies conditions that both rocks differ in effective viscosity and Pennacchioni and Mancktelow (2007) argued that this is the explanation for the observed strain concentration close to a boundary between two distinct rheologies.

7. Conclusions

Thin slices of dry Solnhofen limestone were deformed experimentally in the direct shear geometry in a triaxial testing machine at 600 °C, 200 MPa confining pressure at a bulk shear strain rate of $\sim 5 \times 10^{-3}\,s^{-1}$ between rigid forcing blocks. The development of paired zones of high-shear strain parallel to the specimen boundary was observed, with a central zone of low shear strain. Electron backscatter diffraction was used to quantify the patterns of CPO development within and without the localized high-strain zones. CPO development was consistent with a large non-coaxial (shear) strain component in the shear zones and a dominantly flattening deformation with radial extension in the central, low-strain zone.

The strain distribution was interpreted in terms of superimposition of a heterogeneous strain due to flattening normal to the plane of the sample plus a shearing deformation parallel to the planar boundaries of the sample. Flattening deformation with associated lateral extrusion was possible owing to the limited lateral extent of the sample, despite its thinness. The flattening strain was zero adjacent to the forcing blocks, rising to a maximum in the centre of the specimen.

The inhibition of the development of a high-shear strain in the central part of the sample is attributed to the strain hardening that accompanies the enhanced flattening strain developed in the central region. A small amount of strain hardening can be very effective in this respect, owing to the markedly non-linear rheology of Solnhofen limestone under the conditions of temperature and strain rate imposed. Where the flattening strain is low, close to the edges of the limestone slice, there is insufficient strain hardening to prevent the non-coaxial deformation from dominating. This interpretation of the origin of paired shear bands in these experiments was supported by a numerical simulation that reproduced the main features of the strain distribution in the experimental samples.

Complex strain patterns are known to be able to be produced through different types of strain paths developed in spatially distinct parts of zones of crustal transpression. This study shows that these forms of complexity may be further compounded by taking into account rheological variations that may arise with strain.

In a natural shear zone of sufficiently great lateral extent away from free boundary surfaces so that deformation by simple shear is predominant, or in a material displaying no dependence of flow stress on strain, and/or in a material of more linearly viscous rheology, this type of strain partitioning would not be expected.

Acknowledgements

SL-F acknowledges funding from the European Commission under the V Framework Program (Marie Curie Fellowship contract Nr. HPMF-CT-2000-00778). Experimental Officer Robert Holloway provided in invaluable help with the maintenance of the Nimonic-2 testing machine. Sue Treagus is thanked for discussions on strain refraction in rocks and feedback on an earlier version of the manuscript. This work was completed whilst EHR was in receipt of grant support from the Spanish Ministry of Education and Science during a sabbatical visit to the Institute of Earth Sciences "Jaume Almera" in Barcelona (CSIC). This paper benefited from constructive criticism by Scott Giorgis.

We would like to dedicate this paper to the memory of our colleague and friend, the late Martin Casey, and to recognize his many outstanding contributions to understanding the geometry of naturally and experimentally deformed rocks.

References

Beaumont, C., Jamieson, R.A., Nguyen, M.H., Lee, B., 2002. Himalayan tectonics explained by extrusion of a low-viscosity crustal channel coupled to focused surface denudation. Nature 414, 738–742.

Bestmann, M., Kunze, K., Matthews, A., 2000. Evolution of a calcite marble shear zone complex on Thassos Island, Greece: microstructural and textural fabrics and their kinematic significance. Journal of Structural Geology 22 (11–12), 1789–1807.

Casey, M., 1980. Mechanics of shear zones in isotropic dilatant materials. Journal of Structural Geology 2 (1–2), 143–147.

Covey-Crump, S.J., 1992. Application of a state variable description of inelastic deformation to geological materials. Unpublished PhD Thesis, University Collegue London.

De Bresser, J.H.P., Spiers, C.J., 1997. Strength characteristics of the r, f, and c slip systems in calcite. Tectonophysics 272 (1), 1–23.

Dell'Angelo, L.N., Tullis, J., 1989. Fabric development in experimentally sheared quartzites. Tectonophysics 169, 1–21.

Dewey, J.F., Holdsworth, R.E., Strachan, R.A., 1998. Transpression and transtension zones. In: Holdsworth, R.E., Strachan, R.A., Dewey, J.F. (Eds.), Continental Transpressional and Transtensional Tectonics. Geological Society of London, London, Special Publications, vol. 135, pp. 1–14.

Dresen, G., 1991. Stress-distribution and the orientation of Riedel shears. Tectonophysics 188 (3–4), 239–247.

Gu, Y.J., Wong, T.F., 1994. Development of shear localization in simulated quartz gouge – effect of cumulative slip and gouge particle-size. Pure and Applied Geophysics 143 (1–3), 387–423.
Herwegh, M., Kunze, K., 2002. The influence of nano-scale second-phase particles on deformation of fine grained calcite mylonites. Journal of Structural Geology 24 (9), 1463–1478.
Jaeger, J.C., Cook, N.G.W., 1976. Fundamentals of Rock Mechanics. Science Paperback, London.
Jones, R.R., Holdsworth, R.E., Bailey, W., 1997. Lateral extrusion in transpression zones: the importance of boundary conditions. Journal of Structural Geology 19 (9), 1201–1218.
Llana-Fúnez, S., Rutter, E.H., 2005. Distribution of non-plane strain in experimental compression of short cylinders of Solnhofen limestone. Journal of Structural Geology 27, 1205–1216.
Logan, J., Dengo, C., Higgs, N., Wang, Z., 1992. Fabrics of experimental fault zones: their development and relationship to mechanical behaviour. In: Evans, B., Wong, T.-F. (Eds.), Fault Mechanics and Transport Properties of Rocks. International Geophysics Series, vol. 51. Academic Press Ltd, London, pp. 33–67.
Mancktelow, N.S., Pennacchioni, G., 2005. The control of precursor brittle fracture and fluid – rock interaction on the development of single and paired ductile shear zones. Journal of Structural Geology 27, 645–661.
Mariani, E., 2002. An experimental study of the deformation of white mica. Unpublished PhD Thesis, University of Manchester.
Mariani, E., Brodie, K.H., Rutter, E.H., 2006. Experimental deformation of muscovite shear zones at high temperatures under hydrothermal conditions and the strength of phyllosilicate-bearing faults in nature. Journal of Structural Geology 28 (9), 1569–1587.
Passchier, C.W., Trouw, R.A.J., 1996. Microtectonics. Springer-Verlag, Berlin, Germany.
Pennacchioni, G., Mancktelow, N.S., 2007. Nucleation and initial growth of a shear zone network within compositionally and structurally heterogeneous granitoids under amphibolites facies conditions. Journal of Structural Geology 29, 1757–1780.
Post, A., Tullis, J., 1999. A recrystallized grain size piezometer for experimentally deformed feldspar aggregates. Tectonophysics 303 (1–4), 159–173.
Prior, D.J., Boyle, A.P., Brenker, F., Cheadle, M.C., Day, A., Lopez, G., Peruzzo, L., Potts, G.J., Reddy, S., Spiess, R., 1999. The application of electron backscatter diffraction and orientation contrast imaging in the SEM to textural problems in rocks. American Mineralogist 84 (11/12), 1741–1759.
Ramsay, J.G., Graham, R.H., 1970. Strain variation in shear belts. Canadian Journal of Earth Sciences 7 (3), 786–813.
Ramsay, J.G., Huber, M.I., 1983. The Techniques of Modern Structural Geology. Academic Press, London.
Ramsay, J.G., Huber, M.I., 1987. The Techniques of Modern Structural Geology. Academic Press, London.
Robin, P.Y.F., Cruden, A.R., 1994. Strain and vorticity patterns in ideally ductile transpression zones. Journal of Structural Geology 16 (4), 447–466.
Robinson, D., 1971. The inhibiting effect of organic carbon on contact metamorphic recrystallization of limestones. Contributions to Mineralogy and Petrology 32, 245–250.
Rutter, E.H., 1972. The influence of interstitial water on the rheological behaviour of calcite rocks. Tectonophysics 14, 13–33.
Rutter, E.H., Casey, M., Burlini, L., 1994. Preferred crystallographic orientation development during the plastic and superplastic flow of calcite rocks. Journal of Structural Geology 16 (10), 1431–1446.
Sanderson, D.J., Marchini, W.R.D., 1984. Transpression. Journal of Structural Geology 6 (5), 449–458.
Schmid, S.M., Boland, J.N., Paterson, M.S., 1977. Superplastic flow in finegrained limestone. Tectonophysics 43, 257–291.
Schmid, S.M., Casey, M., 1986. Complete fabric analysis of some commonly observed quartz c-axis patterns. In: Hobbs, B.E., Heard, H.C. (Eds.), The Paterson Volume. Mineral and Rock Deformation: Laboratory Studies. American Geophysical Union Monographs, vol. 36, pp. 263–286.
Schmid, S.M., Panozzo, R., Bauer, S., 1987. Simple shear experiments on calcite rocks: rheology and microfabric. Journal of Structural Geology 9 (5/6), 747–778.
Schreurs, G., Colletta, B., 1998. Analogue modelling of faulting in zones of continental transpression and transtension. In: Holdsworth, R.E., Strachan, R.A., Dewey, J.F. (Eds.), Continental Transpressional and Transtensional Tectonics. Geological Society of London, London, Special Publication, vol. 135, pp. 59–79.
Shimamoto, T., Logan, J.M., 1981. Effects of simulated fault gouge on the sliding behavior of Tennessee sandstone – non-clay gouges. Journal of Geophysical Research 86 (B4), 2902–2914.
Treagus, S.H., 1981. A theory of stress and strain variations in viscous layers, and its geological implications. Tectonophysics 72 (1–2), 75–103.
Treagus, S.H., 1988. Strain refraction in layered systems. Journal of Structural Geology 10 (5), 517–527.
Treagus, S.H., 1993. Flow variations in power-law multilayers – implications for competence contrasts in rocks. Journal of Structural Geology 15 (3–5), 423–434.
Treagus, S.H., Sokoutis, D., 1992. Laboratory modeling of strain variation across rheological boundaries. Journal of Structural Geology 14 (4), 405–424.
Walker, A.N., Rutter, E.H., Brodie, K.H., 1990. Experimental study of grain-size sensitive flow of synthetic, hot-pressed calcite rocks. In: Knipe, R.J., Rutter, E.H. (Eds.), Deformation Mechanisms, Rheology and Tectonics. Geological Society Special Publication, vol. 54, pp. 259–284.